Circulation and Soil Moisture Contributions to Heatwaves in the United States

RUSSELL L. HOROWITZ,[a] KAREN A. MCKINNON,[a,b,c] AND ISLA R. SIMPSON[d]

[a] *Institute of Environment and Sustainability, University of California, Los Angeles, Los Angeles, California*
[b] *Department of Statistics, University of California, Los Angeles, Los Angeles, California*
[c] *Department of Atmospheric and Oceanic Sciences, University of California, Los Angeles, Los Angeles, California*
[d] *Climate and Global Dynamics Laboratory, National Center for Atmospheric Research, Boulder, Colorado*

(Manuscript received 23 February 2021, in final form 29 August 2022)

ABSTRACT: Extreme heat events are a threat to human health, productivity, and food supply, so understanding their drivers is critical to adaptation and resilience. Anticyclonic circulation and certain quasi-stationary Rossby wave patterns are well known to coincide with heatwaves, and soil moisture deficits amplify extreme heat in some regions. However, the relative roles of these two factors in causing heatwaves is still unclear. Here we use constructed circulation analogs to estimate the contribution of atmospheric circulation to heatwaves in the United States in the Community Earth System Model version 1 (CESM1) preindustrial control simulations. After accounting for the component of the heatwaves explained by circulation, we explore the relationship between the residual temperature anomalies and soil moisture. We find that circulation explains over 85% of heatwave temperature anomalies in the eastern and western United States but only 75%–85% in the central United States. In this region, there is a significant negative correlation between soil moisture the week before the heatwave and the strength of the heatwave that explains additional variance. Further, for the hottest central U.S. heatwaves, positive temperature anomalies and negative soil moisture anomalies are evident over a month before heatwave onset. These results provide evidence that positive land–atmosphere feedbacks may be amplifying heatwaves in the central United States and demonstrate the geographic heterogeneity in the relative importance of the land and atmosphere for heatwave development. Analysis of future circulation and soil moisture in the CESM1 Large Ensemble indicates that, over parts of the United States, both may be trending toward greater heatwave likelihood.

KEYWORDS: North America; Atmosphere–land interaction; Extreme events; Temperature; Climate models

1. Introduction

Extreme heat events are a threat to human health and quality of life. Positive temperature extremes increase human mortality and morbidity (Ye et al. 2012; Honda et al. 2014; Romero-Lankao et al. 2014; Gasparrini et al. 2015; Song et al. 2017) and decrease workplace and school productivity (Kjellstrom et al. 2009; Heal and Park 2016; Goodman et al. 2018). Further, our food supply can be damaged by crop exposure to extreme heat (Schlenker and Roberts 2009; Sánchez et al. 2014; Vogel et al. 2019).

Unfortunately, extreme heat is expected to occur more and more frequently as global temperatures increase. For example, between 1986 and 2016, more than twice as many high-temperature records were set in the United States as low-temperature records (Vose et al. 2017). It is therefore increasingly important to understand the physical drivers underlying these dangerous events. Improved prediction and modeling of the underlying factors and the resulting heatwaves may allow for better adaptation to lessen their negative impact on society.

Links between large-scale atmospheric circulation and summer heat extremes are well established. Heatwaves are strongly associated with anticyclonic circulation that leads to subsidence and clear skies that support heating (Meehl and Tebaldi 2004; Gershunov et al. 2009; Pfahl and Wernli 2012; Grotjahn et al. 2016; Adams et al. 2021). In some cases, these anticyclones are associated with quasi-stationary Rossby waves, which have been shown to cause extreme and long-lasting heat events (Schubert et al. 2011; Screen and Simmonds 2014; Röthlisberger et al. 2019), at times inducing co-occurring extremes around the midlatitudes (Coumou et al. 2014; Kornhuber et al. 2019). Horizontal advection of warm air can also play a role in extreme heat development (Lau and Nath 2012; Loikith and Broccoli 2012; Horton et al. 2016; Thomas et al. 2020), where the relevant source of the warm air depends on the location of the heatwave. For example, Yang et al. (2019) found associations with terrestrial warm air advection in the northern United States and with oceanic warm air advection in the southern United States. While these studies have identified co-occurrence of heatwaves with specific circulation patterns, they do not quantify the relative role of circulation versus other processes in causing heatwaves.

In addition to the influence of large-scale circulation patterns, summer temperature extremes can be amplified or damped due to interactions with the land surface. In particular, soil moisture has been identified as an important mediator of interactions between the land surface and the atmosphere (Seneviratne et al. 2010, 2013; Grotjahn et al. 2016; Horton et al. 2016; Lo et al. 2017). Reductions in soil moisture can reduce the latent heat response to incoming energy, thereby warming the surface and increasing the sensible heat flux and

Supplemental information related to this paper is available at the Journals Online website: https://doi.org/10.1175/JCLI-D-21-0156.s1.

Corresponding author: Karen McKinnon, kmckinnon@ucla.edu

DOI: 10.1175/JCLI-D-21-0156.1

© 2022 American Meteorological Society. For information regarding reuse of this content and general copyright information, consult the AMS Copyright Policy (www.ametsoc.org/PUBSReuseLicenses).

Unauthenticated | Downloaded 11/29/22 04:04 PM UTC

lower-atmospheric temperatures (Fischer et al. 2007b; Miralles et al. 2014). The reduction in evapotranspiration can further increase temperatures by causing reduced cloud cover and decreased precipitation (Miralles et al. 2019; Selten et al. 2020).

Soil moisture deficits have been linked to specific extreme heat events in the United States and Europe (Fischer et al. 2007a; Hauser et al. 2016; Wehrli et al. 2019), and multiple studies have performed simulations with and without interactive soil moisture to show that land–atmosphere interactions amplify heatwaves (Lorenz et al. 2010; Jaeger and Seneviratne 2011; Stéfanon et al. 2014; Vogel et al. 2017). Focusing on the atmospheric response, Merrifield et al. (2019) performed a modeling experiment constraining circulation at different levels to demonstrate that heatwaves are intensified by land surface–atmosphere interactions. While these studies have quantified the influence of soil moisture in idealized settings and/or for individual events, we are lacking a more general diagnostic analysis of the relative roles of the atmosphere and the land surface in causing extreme heat.

Understanding the relative importance of soil moisture in heatwave development is especially worthwhile because of its potential predictive capacity. Soil moisture provides a memory of previous land–atmosphere conditions (Koster and Suarez 2001; Seneviratne et al. 2006), whereas the atmosphere is inherently chaotic and difficult to predict beyond short time scales. Antecedent precipitation, through its effect on soil moisture, has been identified as a predictor of heatwaves in some regions (Hirschi et al. 2011; Mueller and Seneviratne 2012; McKinnon et al. 2016). Therefore, quantifying the role soil moisture plays in extreme heat events across broad geographies may enhance our ability to predict heatwaves in the future.

Here, we take a unified approach to exploring the contribution of atmospheric circulation versus other processes to heatwaves in nine climate regions of the continental United States using control simulations from version 1 of the Community Earth System Model (CESM1; Hurrell et al. 2013). CESM1 compares well to historical extreme temperature metrics (Sillmann et al. 2013) and global near-surface temperature trends (Hurrell et al. 2013). We estimate the contribution of circulation to temperature anomalies through dynamical adjustment using constructed circulation analogs (Deser et al. 2016), which have been applied successfully to monthly temperatures during winter (Deser et al. 2016; Lehner et al. 2017) and summer (Merrifield et al. 2017). The analysis is performed on a daily time scale, which allows us to quantify the impact of circulation on extreme heat events. We can then identify regions where there is amplification of temperatures during heatwaves above what is estimated by the constructed circulation analogs and explore whether soil moisture plays a role in this amplification. Finally, we examine projected changes in the identified heatwave components—atmospheric circulation and soil moisture—in the CESM1 Large Ensemble (Kay et al. 2015).

The rest of the study is presented as follows. Section 2 describes the CESM1 datasets used and summarizes the constructed circulation analog technique, along with the modifications we made to apply it to daily data. Section 3 shows the results of the dynamical adjustment and identifies future trends. The results and implications are discussed in section 4.

2. Data and methods

a. The CESM1 control simulations and large ensemble

We use data from simulations conducted with version 1 of the Community Earth System Model (CESM1) at a nominal 1° resolution. Two preindustrial control simulations are used, both with forcings representative of the year 1850. The primary dataset analyzed is a fully coupled preindustrial control run (PiCTL). The simulation was previously completed by the National Center for Atmospheric Research and run for 1799 years. We use all years from this PiCTL simulation in our analysis. This is compared with a 2600-yr preindustrial control run, of which only the first 1799 years are used, where sea surface temperatures are prescribed to those of the seasonally varying monthly climatology from PiCTL (fixSST-PiCTL).

Future projections are from the CESM1 Large Ensemble (CESM1-LE; Kay et al. 2015). This consists of 40 ensemble members that have the same radiative forcing, but slightly perturbed initial atmospheric conditions, allowing internal variability to lead to a range of possible outcomes (Deser et al. 2016). The ensemble members differ only in a very small round-off error to the initial air temperature on 1 January 1920. These runs are forced by historical radiative forcing from 1920 to 2005 and then by RCP8.5 radiative forcing until 2100 (Taylor et al. 2012).

We use daily average 2-m air temperature (hereinafter simply temperature), sea level pressure, surface latent heat flux, surface sensible heat flux, 500-hPa geopotential height, and soil moisture in the top 10 cm of soil for our analysis. The climatological mean and seasonal cycle of each variable at each grid box are removed by projecting the time series onto the first three annual harmonics, then subtracting the fitted values. All of our analyses are based on the anomalies from the seasonal cycle. We focus on the summer season, June–August (JJA), in the continental United States, which is split into the nine climate regions identified by Karl and Koss (1984). These climate regions are identified in Fig. 1a. While each region is analyzed separately, some figures presented in this paper will combine the results from all regions into a single map.

b. Constructed circulation analogs for daily data

To calculate the daily dynamical component of the temperature anomalies in each region, we implement constructed circulation analogs (CCAs; Deser et al. 2016). A brief summary of the CCA method, with modifications made for this study, follows. To estimate the dynamical contribution to temperature anomalies for a target day in a given region, we begin with the sea level pressure (SLP) anomalies from the prior day, which we will refer to as the lead-1 SLP anomalies. We use the lead-1 SLP anomalies to reduce the influence of temperature on SLP, although we note that the lead time does not entirely prevent this influence, given the persistence and coupled nature of the system. The SLP anomalies come from a larger spatial domain than the climate region whose temperature is of

Unauthenticated | Downloaded 11/29/22 04:04 PM UTC

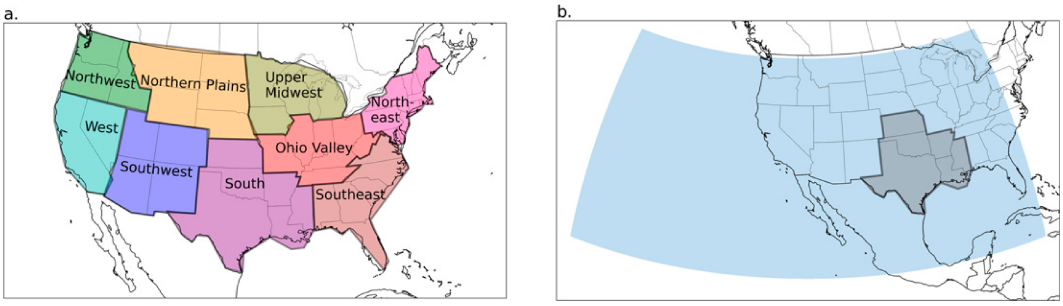

FIG. 1. (a) The nine climate regions used in this analysis (Karl and Koss 1984), and (b) the South region, in gray, and its broader sea level pressure region, in blue, used for the constructed circulation analogs.

interest. For each region, we select an area that extends 54° west, 18° east, 15° north, and 15° south of the center of the region. This domain is chosen to span the wavelength of a zonal wavenumber-5 pattern in the longitude direction. Patterns with zonal wavenumber 5, as well as wavenumbers 6 and 7, have been associated with summer temperature extremes in North America (Teng et al. 2013; Screen and Simmonds 2014; Kornhuber et al. 2020), so choosing a domain of this size will capture patterns of wavenumber 5 and higher. An example of this broader SLP region relative to the specific region of interest is shown in Fig. 1b.

For each target day and region, we next identify SLP anomaly analogs that closely match the lead-1 SLP anomaly pattern from the target day. The analogs may come from N_y years in the same preindustrial control simulation, which cannot include the same year as the target day. The maximum value for N_y is therefore 1798 years, 1 year less than the total length of the control simulation, and we explore the effect of decreasing N_y below. To account for the differing seasonal effects of circulation on temperature, only days between 1 week before and 1 week after the day of summer being analyzed are allowed as potential analogs. The importance of this constraint is shown in Fig. 2. Although we have removed the seasonal cycle in SLP and temperature, the temporal standard deviation of SLP, averaged across the broader wave-5 domain, and temperature, averaged across the regions of interest, is not stationary throughout the summer. The standard deviation of SLP decreases in June and July and increases in August in all regions and both increasing and decreasing trends across the summer are present for temperature standard deviation. It is therefore reasonable to expect that the same SLP anomaly pattern in June and August may produce different temperature responses, which will be limited by placing the 2-week restriction on analogs. This restriction means that for any given day, there are 15 days from each of the N_y years that can potentially be used as analogs, but no more than one day per year is selected so as to eliminate the risk of selecting multiple analogs from the same circulation event.

After specifying the pool of potential analogs, we identify the N_a closest options as measured by the lowest Euclidean distance to the target lead-1 SLP anomalies. To reduce the noise in our method, we subsample N_s analogs from our set of N_a options without replacement to generate the dynamical component.

Using these N_s analogs, ordinary least squares regression is performed to obtain the weights $\boldsymbol{\beta}$ of the analogs to match the target lead-1 SLP field according to

$$\mathbf{S}_t = \mathbf{S}_s\boldsymbol{\beta} + \boldsymbol{\epsilon}, \tag{1}$$

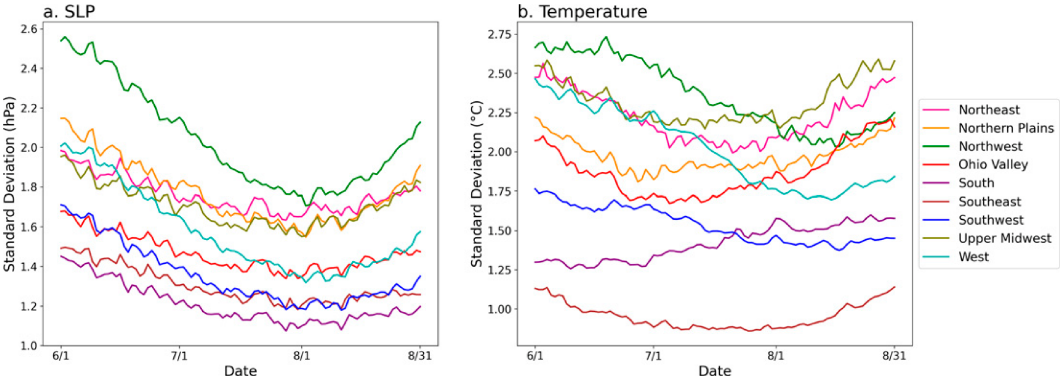

FIG. 2. The area-weighted standard deviation of (a) sea level pressure anomalies and (b) temperature anomalies across all years of the fully coupled preindustrial control simulation for each date of the summer. The sea level pressure anomaly is an area-weighted average over the entire spatial domain used in the constructed circulation analogs, whereas the temperature anomaly is an area-weighted average over only the region of interest.

Unauthenticated | Downloaded 11/29/22 04:04 PM UTC

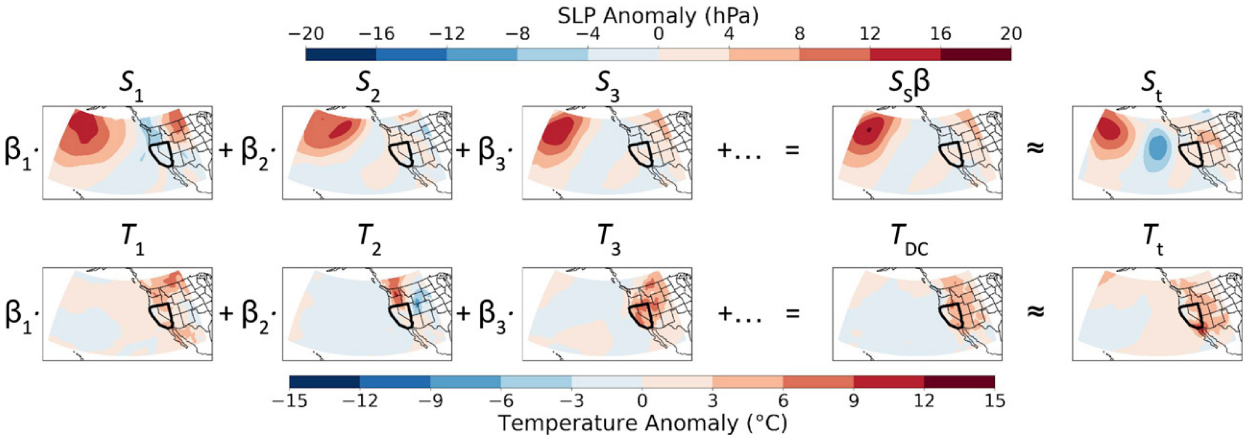

FIG. 3. A schematic showing the constructed circulation analog approach for a single day for the West region (outlined in black). The top row shows how the SLP analog patterns (three examples, $\mathbf{S}_{1\ldots3}$; shown) combine to produce the constructed circulation analog $\mathbf{S}_s\boldsymbol{\beta}$, which resembles the target pattern $\mathbf{S}_t$. The $\boldsymbol{\beta}$ parameters learned from the regression on the SLP patterns are applied to the associated temperature patterns to produce the dynamical component of temperature $\mathbf{T}_{dc}$. Note that, for our use of constructed circulation analogs, the SLP patterns lead the temperature patterns by 1 day.

where $\mathbf{S}_t$ is an $m \times 1$ column vector with the target lead-1 SLP anomalies, m is the number of grid points in the pattern, $\mathbf{S}_s$ is an $m \times N_s$ matrix in which each column contains the SLP anomalies from one of the N_s analogs, and ϵ is the residual. We do not subset the domain in any way before performing the regression; implications of this choice are discussed later in the paper. The resulting $\boldsymbol{\beta}$ is an $N_s \times 1$ column vector of weights for each of the analogs. These weights are then applied to the temperature anomalies that follow each analog by one day to estimate the dynamical contribution to the target day's temperature anomalies at each grid cell in the region according to

$$\mathbf{T}_{dc} = \mathbf{T}_s\boldsymbol{\beta}, \tag{2}$$

where $\mathbf{T}_{dc}$ is an $m \times 1$ column vector containing the estimated temperature anomalies (the dynamical component) for the target day, $\mathbf{T}_s$ is the $m \times N_s$ matrix where each column is the temperature anomaly 1 day after each of the N_s SLP anomaly analogs, and $\boldsymbol{\beta}$ is calculated from Eq. (1).

This is repeated N_r times, with the final dynamical component estimated as the mean estimated dynamical component of all N_r samples following Deser et al. (2016). We vary both the number of repeated samples and the number of analog years to assess the sensitivity of the results to these values (section 3a). For our primary analysis, we use the same values as Deser et al. (2016) for $N_a = 150$ and $N_s = 100$, as well as $N_r = 20$ and the maximal value of $N_y = 1798$.

The process of CCA for a single day is shown in Fig. 3. The top row shows a subset of the selected SLP analogs $\mathbf{S}_{1\ldots3}$ that are linearly combined (with the other 97 analogs; not shown) to produce an SLP anomaly pattern $\mathbf{S}_s$ that closely (but not exactly) resembles the target pattern $\mathbf{S}_t$. The $\boldsymbol{\beta}$ coefficients estimated in Eq. (1) (shown in the top row of the schematic) are then applied to the corresponding temperature fields that lag SLP by one day to produce the dynamical component of temperature, $\mathbf{T}_{dc}$. In this case, the dynamical component of temperature in the West is very similar to the actual temperature anomalies, with overall positive anomalies that are maximized in the southern and northeastern parts of the domain. This process is applied to each day of the control simulation independently.

3. Results

a. Daily CCA performance

Although the focus of this paper is on heat extremes, we are also interested in the performance of dynamical adjustment on daily time scales, because most previous work has focused on monthly or seasonal temperature averages. Deser et al. (2016) showed that when using CCAs for winter temperature over North America, the average root-mean-square error (RMSE) converged with N_r less than 20. Here, we vary N_y, the number of analog years, and N_r, the number of subsamples averaged over each analog selection. Then we calculate the average RMSE for temperature anomalies for each region and over the entire continental United States for summer. The sensitivity of RMSE to N_r, in Fig. 4a, is very similar to that found by Deser et al. (2016). The thick black line indicates the RMSE over the entire continental United States, while the colored lines show the results for all regions. Increasing N_r, while keeping N_y constant at its maximum value of 1798, results in average summer RMSE declining approximately exponentially, but plateauing before $N_r = 20$, which is the value used in this analysis. All regions follow a very similar pattern of exponential decline. The main difference between regions is the value at which they plateau. Regions with greater variability in summer temperature will tend to have greater RMSE values, as will regions where SLP is less related to temperature variation. Many of these regional differences in the performance of the CCAs hold when looking at heatwaves as well and will be discussed more below.

Unauthenticated | Downloaded 11/29/22 04:04 PM UTC

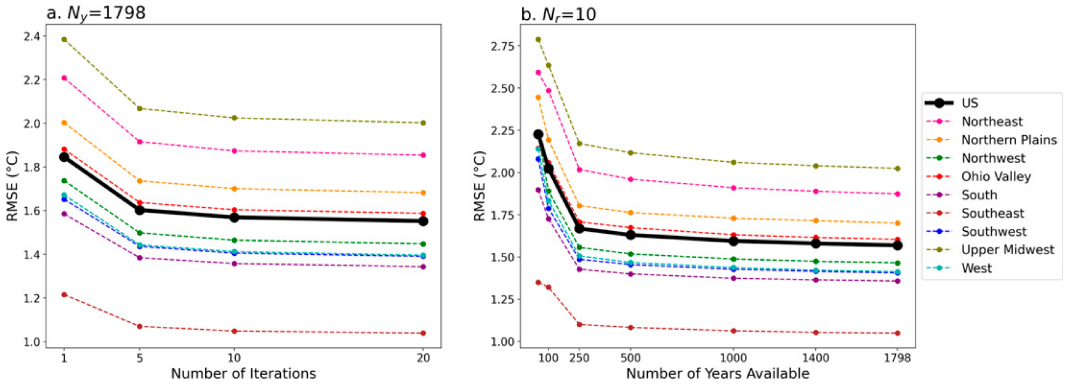

FIG. 4. The area-weighted root-mean-square error (RMSE) for summer temperature averaged in the continental United States (black) and each climate region (colors) for the fully coupled preindustrial control simulation. Constructed circulation analogs are performed with varying (a) N_r, with N_y set at 1798, and (b) N_y, with N_r set at 10; N_r is the number of iterations of the constructed circulation analog procedure that is performed and averaged for each day, and N_y is the number of years of analogs from which to select.

Figure 4b shows the sensitivity of RMSE to the number of years of analogs, with N_r kept constant at 10; N_y is varied from 50 years to 1798 years. The RMSE again appears to decrease exponentially, roughly converging after more than 500 years are available. This seems to indicate that results for this analysis would not be substantially different with a longer preindustrial control run. However, this has important implications for working with observations, where many fewer analogs are available. Daily CCAs may perform poorly if too few sufficiently close analogs exist.

b. *Heatwaves and CCA results*

Candidate heatwaves for each region are defined as the hottest consecutive 7-day period in each summer, averaged over all grid cells, area-weighted, in each region. Heatwaves are defined based on temperature anomalies, rather than absolute temperatures. An anomaly-based definition reflects the fact that humans tend to be most sensitive to deviations from an expected baseline (e.g., Guirguis et al. 2014; Moore et al. 2019), but it should be noted that a given heatwave is not necessarily the hottest week in absolute temperatures each year. Each of these heatwaves has an associated dynamical component that has been estimated from the CCAs. This dynamical component is interpreted as the expected contribution of atmospheric circulation to the heatwave. Since we are selecting weeks that are abnormally hot, the average dynamical component from all heatwaves will be greater than zero. However, this definition assumes that there is a heatwave during every summer, so many weeks that fit this criterion are not particularly extreme. Therefore, only those heatwaves with an estimated dynamical component in the 85th percentile or greater are analyzed, leaving us with 270 heatwaves per region across the full control simulation. It is these events that we will refer to as heatwaves in the remainder of this study. Filtering in this manner isolates events with a circulation pattern that is expected to be associated with extreme heat.

The residual component of the temperature anomaly during each heatwave, calculated as the actual temperature anomaly minus the dynamical component, is unexplained by the linear relationship with lead-1 SLP anomalies that is captured with the CCA methodology. Any influence of land surface preconditioning, the prior time evolution of the circulation leading up to the heatwave, and/or nonlinear circulation–temperature relationships will be present in this residual. Our aim is to dissect the residual to explore the influence of land–atmosphere coupling during events with a similarly extreme dynamical contribution.

Mean temperature anomalies during the heatwave weeks from PiCTL are displayed in Fig. 5a. Temperature anomalies are highest in the Northwest, reaching up to 6.5°C in the northwestern part of the region, with a regional average anomaly of 4.3°C. The West and most of the northern regions (Northern Plains, Upper Midwest, Ohio Valley, and Northeast) have more moderate extreme heat weeks, with regional averages ranging between 3.1° and 4.1°C, while the southern regions (Southeast, South, and Southwest) have smaller anomalies, between 1.6° and 3.0°C. Figure 5b displays the intraseasonal standard deviation of temperature during the summer in PiCTL, calculated as the square root of the average variance of daily temperatures during each summer. The pattern of heatwave magnitude in Fig. 5a generally follows this spatial pattern in summer temperature standard deviation, but with some important differences. Both heatwave magnitude and standard deviation tend to increase from south to north, with the greatest values in the Northwest and the smallest values in the Southeast. However, the South region and Northern Plains region, particularly over Oklahoma, North Dakota, and South Dakota, stand out as areas where the average heatwave magnitude is greater than one might expect from the summer temperature standard deviation.

The temperature anomalies associated with the heatwaves are qualitatively similar in the fixSST-PiCTL control simulation (Fig. S1 in the online supplemental material), indicating the dominance of atmospheric and land processes in controlling the statistics of the heatwaves. Three regions, the Southwest, Upper Midwest, and Northern Plains, show a slightly

Unauthenticated | Downloaded 11/29/22 04:04 PM UTC

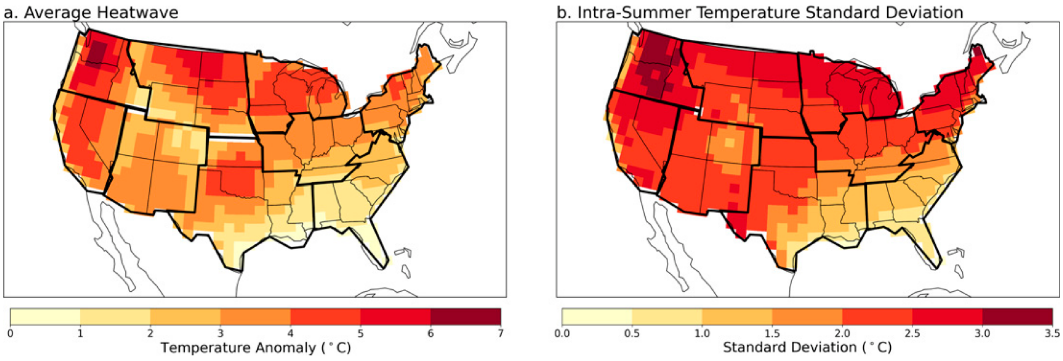

FIG. 5. In the fully coupled preindustrial control simulation, (a) average temperature anomalies during heatwaves and (b) daily summer temperature standard deviation, calculated as the square root of the average of the variances calculated for each summer individually.

larger anomaly in PiCTL than fixSST-PiCTL by between 0.1° and 0.2°C, while differences for all other regions are between −0.1° and 0°C. Given the overall small differences between PiCTL and fixSST-PiCTL, we present results using only the fully coupled control simulation in the main text.

Although some regions have spatial homogeneity in the average temperature anomaly during heatwaves, a number of regions have spatial variation that could affect results when analyzing the region as one unit or be indicative of poor regional grouping. In particular, the South region is more extreme in its northern portion, and the eastern Northwest/western Northern Plains are less extreme than the rest of those regions. It is possible that we see these differences because certain parts of a region do in fact experience less-extreme temperatures during heatwaves or that the region experiences spatially asynchronous heatwaves. Since a heatwave is defined as the hottest 7-day period during the summer over the entirety of a region, a single event could occur more strongly in one part of the region than another. This effect is likely removed by averaging over many events, but it is possible that there is a weak association in heatwave temporal occurrence, with one part of the region dominating the most extreme weeks. While not pursued here, an alternative approach to using prespecified climate regions is to use clustering methods to objectively identify regions that experience extreme heat events at the same time (Lau and Nath 2012; McKinnon et al. 2016; Kornhuber et al. 2020).

The average lead-1 SLP anomaly pattern associated with heatwaves for each region is shown in Fig. 6. While the constructed circulation analog associated with each heatwave is calculated independently, the average across the heatwave patterns provides a general overview of the types of circulation that precede heatwaves in each region. Most regions exhibit a boundary between positive and negative SLP anomalies close to or inside of the region. This suggests a role for advection during these events, depending on the orientation of the boundary. For example, the geostrophic flow associated with the Northwest SLP anomalies (Fig. 6a) is southerly, which would bring warm air from the interior west into the region. Likewise, in the Ohio Valley (Fig. 6h) the geostrophic flow would bring warmer air from the southwest. The Southwest and South regions tend to exhibit negative SLP anomalies during heatwaves, likely indicating the presence of thermal lows caused by elevated surface temperatures. The lead-1 SLP anomalies immediately preceding and following heatwaves are shown in Figs. S2 and S3 in the online supplemental material.

The consistency of the lead-1 SLP anomalies for each region is summarized by a signal-to-noise (S2N) ratio, where the signal is defined as the absolute value of the average composite across the heatwave weeks, and the noise is the standard deviation across the individual weeks that are averaged into the composite. The stippling in Fig. 6 indicates grid boxes where the S2N is less than 1. This highlights that the most consistent lead-1 SLP anomalies for a given region tend to either overlap or span (in the case of dipoles) the region. In all cases where the Aleutian low region was included in the domain, these anomalies, while large, are not found to be of a consistent sign across heatwaves; their presence in the composite maps is primarily due to averaging of large-amplitude noise.

Although we use the average plots to summarize the general behavior of SLP in advance of heatwaves, a benefit of the CCA approach is that it does not require the dynamical component for each heatwave to be the same. Rather, the best constructed analog is found separately for each day. Thus, the method allows for the possibility that multiple types of circulation patterns can lead to heatwaves in a given region. To explore this idea further, we use hierarchical agglomerative clustering with the Ward distance (e.g., Kretschmer et al. 2018) to group the lead-1 SLP patterns for each heatwave week into five clusters and show the three clusters that contain the most weeks in Fig. 7. The S2N is stippled in the same manner as in Fig. 6. As expected from Fig. 6, the SLP anomaly patterns near the heatwave region are reasonably similar across clusters, although it is common to see more weight on one or the other of the nodes of the dipoles in a single cluster (e.g., compare the three clusters in the Northeast region). This suggests that the large-scale structures of the heatwave-related circulation patterns are relatively consistent across events. For regions in the western half of the United States, it is notable that the clusters are primarily distinguished by the sign of the SLP anomaly in the North Pacific Ocean (e.g., the

Unauthenticated | Downloaded 11/29/22 04:04 PM UTC

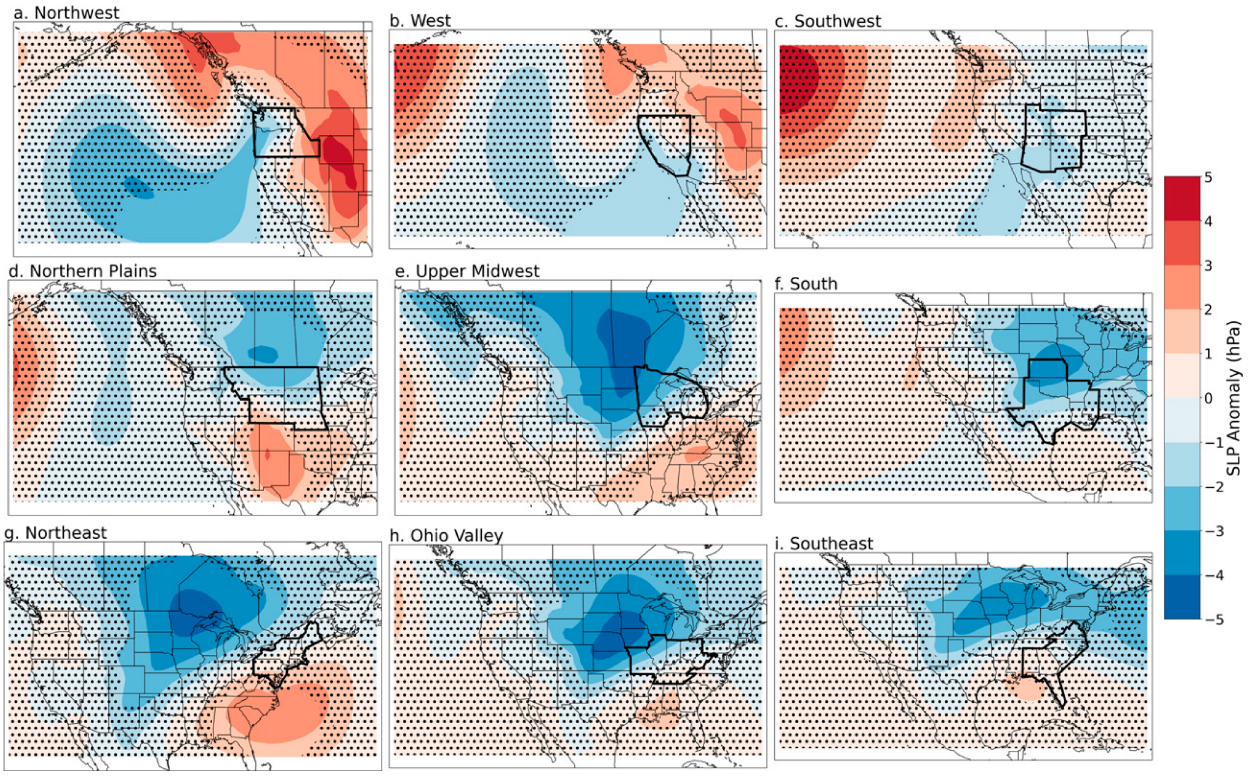

FIG. 6. Average lead-1 sea level pressure anomalies during heatwaves in the fully coupled preindustrial control simulation. The region of interest is outlined in black. The colored area shown is the spatial region used for sea level pressure in the constructed circulation analogs. Stippling indicates a signal-to-noise ratio of <1, where the signal is defined as the absolute value of the average across weeks, and the noise is the standard deviation.

second and third cluster for the West), but the anomalies more proximal to the region of interest tend to be consistent. It is likely that this behavior emerges because of the highly variable nature of SLP in the North Pacific rather than being truly distinct heatwave-causing circulation patterns.

The fact that the most consistent lead-1 SLP anomalies tend to be located close to the region of interest suggests that a smaller domain may be a better choice for dynamically adjusting temperature using lead-1 SLP as the proxy for circulation. Indeed, we find that using a narrower domain that spans a wave-7 sinusoid leads to a small reduction in the RMSE (a range of 3%–9% across regions, with an average of 6%) between the dynamically predicted temperature and actual temperature across heatwave weeks. In contrast, using a larger domain (spanning a wave-4 pattern) leads to a comparable increase in RMSE. Although using a maller domain does lead to a slight reduction in RMSE, we elect to retain our original wave-5 domain given prior work on the length scales of atmospheric circulation for heatwaves in North America (Teng et al. 2013; Screen and Simmonds 2014; Kornhuber et al. 2020).

To further understand the meteorology of these events, we similarly show the average lead-1 500-hPa geopotential height (Z500) anomalies with stippling indicating the S2N ratio in Fig. 8. The lead-1 Z500 anomalies display a more consistent pattern across regions than SLP anomalies, with all regions containing or near the center of a Z500 high, although the magnitudes of the geopotential height anomalies vary substantially. In five of the nine regions (Southwest, Upper Midwest, Northeast, Ohio Valley, and Southeast), an upstream lobe of the wave train also exhibits an S2N > 1, indicating a relatively consistent phasing of the atmospheric anomalies for those heatwaves. Because the Z500 height and the temperature of the atmospheric column are closely linked, these high-Z500 patterns may be both a cause of and a response to the extreme heat. For the former, high atmospheric pressure is associated with clear skies and enhanced solar radiation at the surface; for the latter, Z500 will increase as the atmospheric column warms. While Merrifield et al. (2017) found that Z500 anomalies performed better as an explanatory variable than SLP anomalies in some regions in the United States, we choose to use SLP anomalies as our atmospheric circulation proxy to be consistent with the majority of the CCA literature (Deser et al. 2016; Lehner et al. 2017, 2018).

The average component of the temperature anomaly unexplained by the dynamical prediction from the CCAs for these extreme events is shown in Fig. 9a, and the proportion of the anomaly that is unexplained is displayed in Fig. 9b. Throughout most of the United States, the dynamical component accounts for at least 85% of heatwave temperature anomalies.

Unauthenticated | Downloaded 11/29/22 04:04 PM UTC

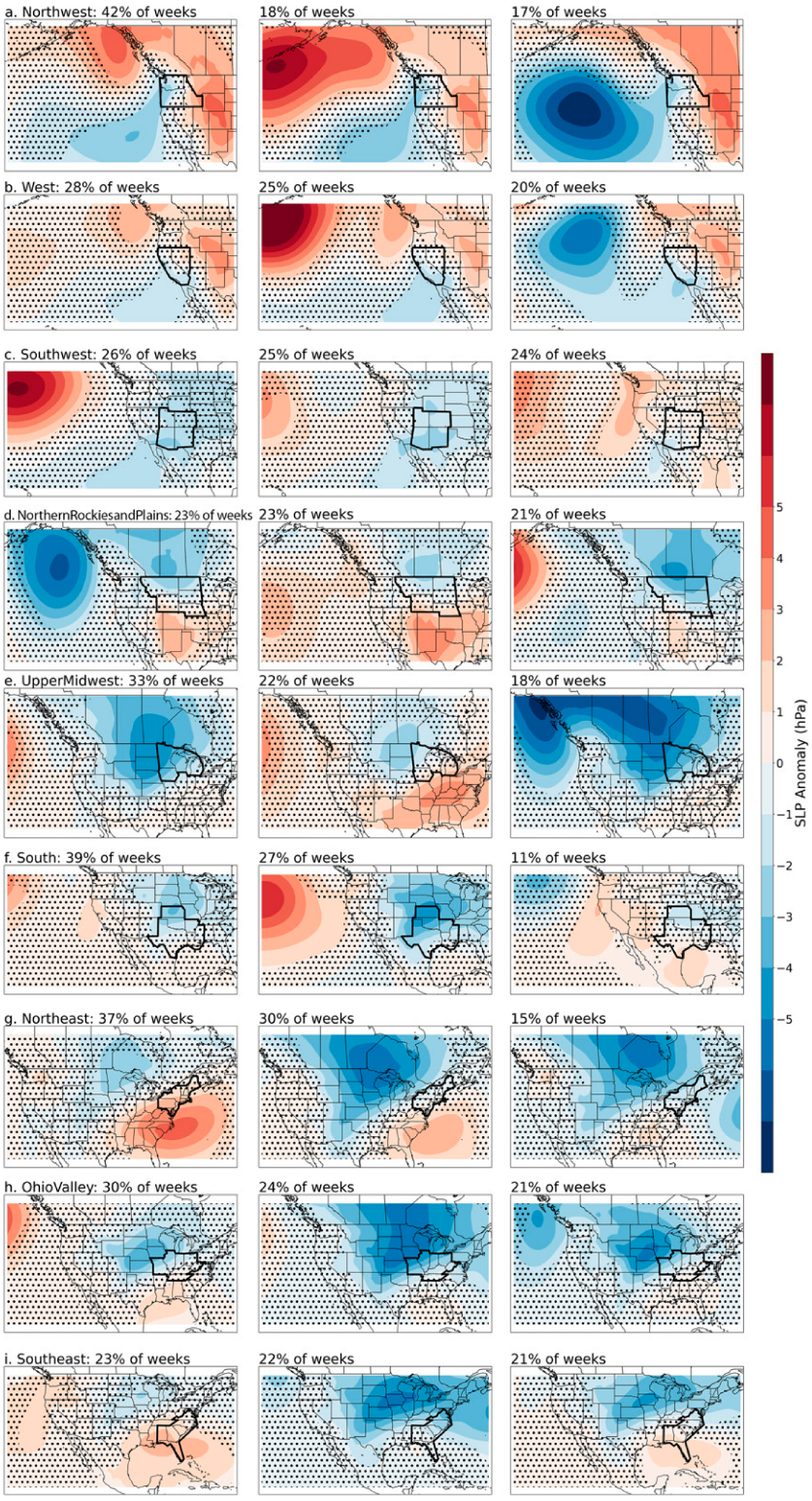

FIG. 7. The most common three clusters (of a total of five) for the lead-1 sea level pressure anomalies in each region. The relevant region is outlined in black. The percentage of heat-wave weeks (of 270) that fall into each cluster is shown in the subtitles. Stippling indicates a signal-to-noise ratio of <1, where the signal is defined as the absolute value of the average across weeks, and the noise is the standard deviation.

Unauthenticated | Downloaded 11/29/22 04:04 PM UTC

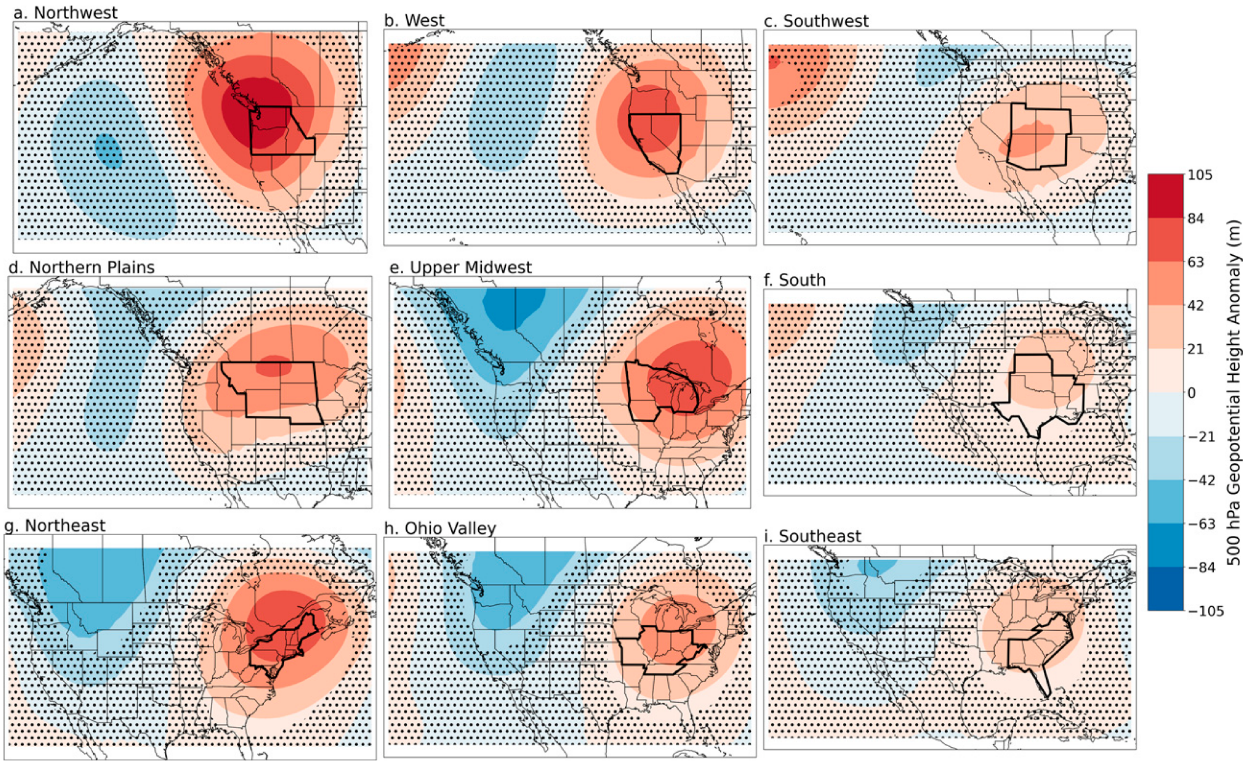

FIG. 8. As in Fig. 6, but for geopotential height anomaly at 500 hPa.

The main exception is in the central United States, which includes the South and Northern Plains climate regions, where greater than 15% of heatwave anomalies are unexplained. This is also true for the Southeast, in Florida, and along the Atlantic coast, but since heatwave anomalies are relatively small in these regions (see Fig. 5a), the magnitude of the residual temperature anomaly is also very small relative to other regions. The central United States stands out as having a larger residual component measured in both temperature anomaly and proportion. We note that using lead-1 SLP anomalies in the dynamical adjustment, as compared with concurrent or lead-3 SLP anomalies, leads to the circulation explaining the largest portion of heatwave temperature anomalies in all regions.

Even in the central United States, the residual component never exceeds 25% of the heatwave anomaly on average. This indicates that, as expected, the largest explanatory factor for extreme heat is atmospheric circulation. This is not to say that temperature tendencies due to atmospheric circulation are the sole driver, but that atmospheric circulation anomalies and the physical processes that accompany these anomalies are the primary cause of extreme heat. Nevertheless, the residual component is important to understand for two reasons. First, inasmuch as it is linked to boundary conditions, it may

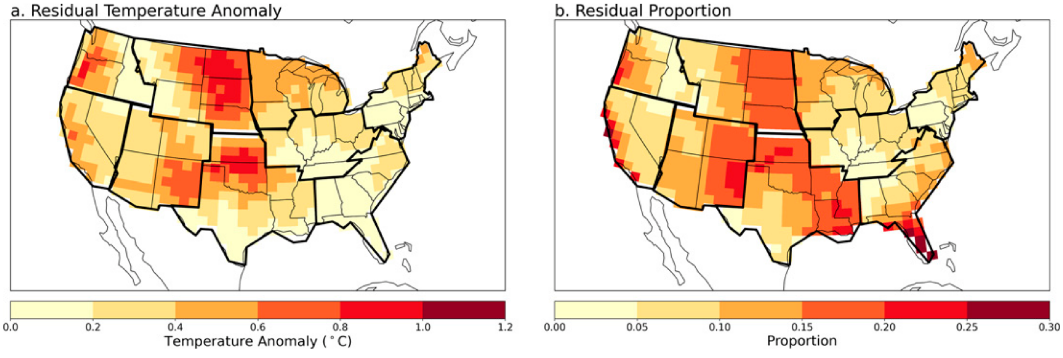

FIG. 9. For heatwaves in the fully coupled preindustrial control simulation, (a) average residual temperature anomalies during heatwaves after removing the average dynamical component from the temperature anomalies and (b) proportion of the average heatwave temperature anomalies accounted for by residual temperature anomalies.

Unauthenticated | Downloaded 11/29/22 04:04 PM UTC

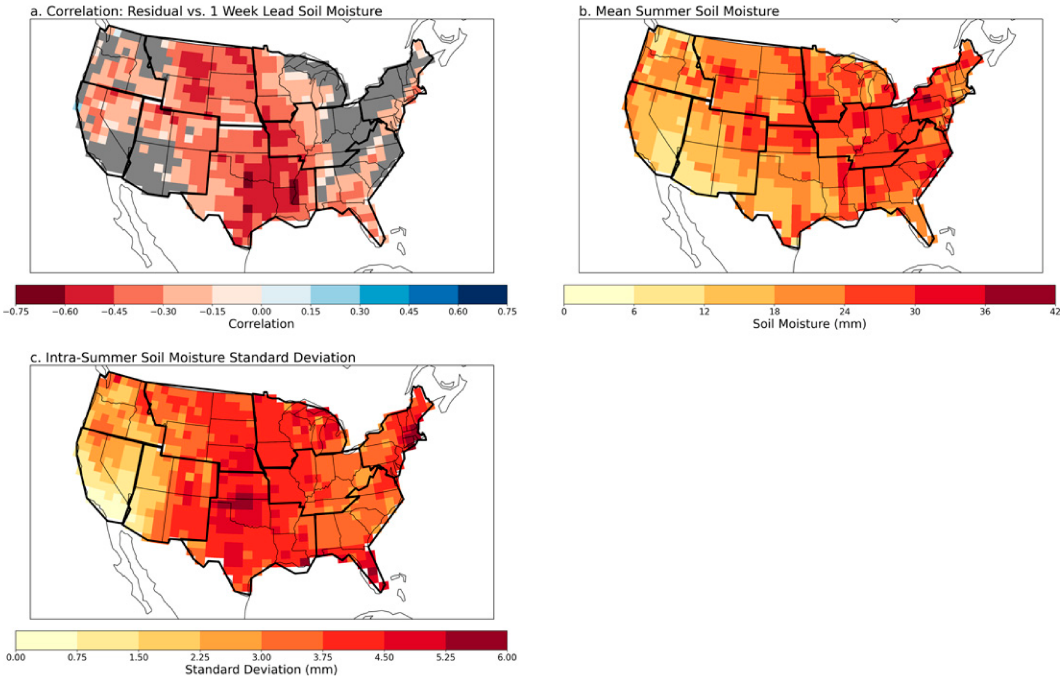

FIG. 10. (a) Correlation between the average residual temperature anomalies during a heatwave and average soil moisture anomalies the week before the heatwave for fully coupled preindustrial control simulation heatwaves. Grid cells that are not significant when controlling for a false discovery rate of 0.05 are gray. (b) Mean summer soil moisture, and (c) daily summer soil moisture standard deviation, calculated as the square root of the average of the variances calculated for each summer individually.

allow for predictability on longer-than-weather time scales (Hirschi et al. 2011; Mueller and Seneviratne 2012; McKinnon et al. 2016). Second, given the nonlinear nature of impacts of extreme heat (e.g., Anderson and Bell 2009; Schlenker and Roberts 2009), the amplification of temperature anomalies by 15%–25%, as seen on average in the central United States, is not inconsequential.

Despite the low proportion of heatwave temperature anomalies explained by the residual component across much of the United States, the average residual component in all grid cells is positive. This implies that heatwaves have both a circulation pattern associated with positive temperature anomalies (a dynamical component greater than zero, by design) and are hotter than circulation alone would predict (a residual component greater than zero), possibly indicating a role for positive land surface feedbacks on the hottest weeks. This is consistent with prior work showing that the land surface tends to amplify, not damp, heat extremes (Lorenz et al. 2010; Jaeger and Seneviratne 2011; Stéfanon et al. 2014; Vogel et al. 2017).

c. *The role of soil moisture*

Motivated by the body of research that identifies soil moisture as an important factor for temperature variability and extremes during summer (Seneviratne et al. 2010, 2013; Grotjahn et al. 2016; Horton et al. 2016; Lo et al. 2017), its impact on the residual component is explored below. The correlation between the residual component and the average soil moisture anomalies in the top 10 cm of soil one week prior to each heatwave is displayed in Fig. 10a. Only those correlations that are significant when controlling for a false discovery rate (Benjamini and Hochberg 1995) of 0.05 are colored. We examine the preceding, rather than synchronous, soil moisture anomalies because heatwaves can both be amplified by and cause low soil moisture; a deficit prior to the heatwave is more suggestive that the heatwave-associated circulation pattern occurred over preconditioned dry soils, although this bidirectional causality cannot be completely resolved. The residual component is significantly negatively correlated with one-week lagged soil moisture anomalies in a large swath of the South and Northern Plains regions, with smaller areas of negative correlations scattered throughout the rest of the country. The area of large negative correlations roughly aligns with areas that have a larger residual proportion in Fig. 9b. In particular, the central United States, with an average correlation of −0.39, and the western portion of the Ohio Valley have greater associations between their residual component and deficits in soil moisture.

The spatial structure of the correlation map is related to the spatial structure in mean and variance of soil moisture. In the western United States, both the mean soil moisture and its intraseasonal standard deviation are small; in these dry regimes, soil moisture anomalies do not typically have an impact on temperature anomalies (Seneviratne et al. 2010). On the east coast,

Unauthenticated | Downloaded 11/29/22 04:04 PM UTC

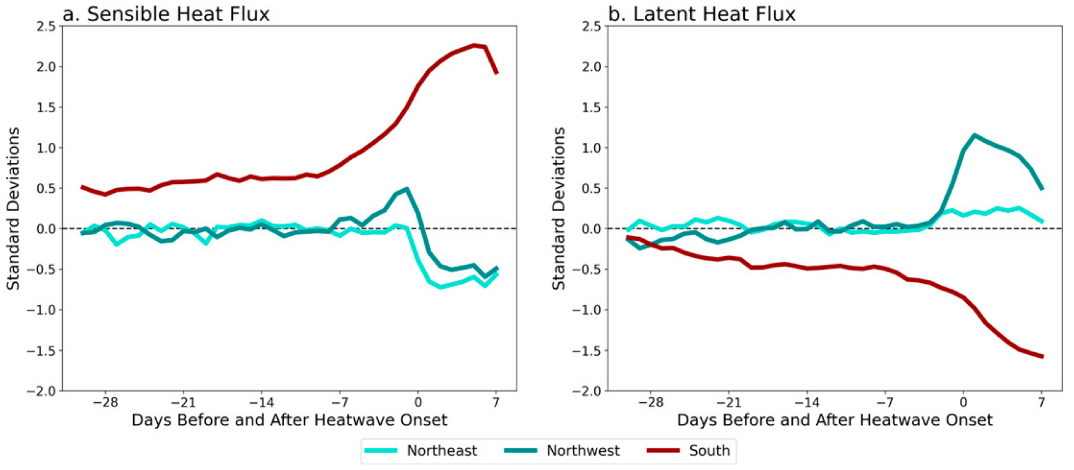

FIG. 11. For heatwaves in the fully coupled preindustrial control simulation in three representative regions, (a) average sensible heat flux anomalies and (b) average latent heat flux anomalies for 31 days before the start of the heatwave (day 1) through the last day of the heatwave (day 7). The fluxes are measured in standard deviations, which have been calculated for each region as the square root of the area-weighted average of the variances calculated for each summer individually. The Northeast and Northwest (blue colors) are chosen to represent energy-limited regions, whereas the South (red) is chosen to represent moisture-limited regions.

although soil moisture variability is greater, the correlation with the residual component is still near zero, consistent with the region being "energy limited" as opposed to "moisture limited" (Teuling et al. 2009). Therefore, we expect variations that alter the radiation reaching the surface, such as cloudiness, to be more important. In contrast, the central United States is a classic transitional region with low enough mean soil moisture to be moisture limited (Vargas Zeppetello et al. 2020) and high soil moisture variability, leading to greater potential for soil moisture variations to alter the surface energy balance and amplify the near-surface temperature.

The difference between moisture-limited and energy-limited regimes is further explored in Fig. 11, which shows the average sensible and latent heat flux anomalies from 31 days prior to the start of a heatwave through the last day of the heatwave. The South climate region is selected to represent the moisture-limited case, whereas the Northwest and Northeast both represent energy-limited regimes. In the South, latent heat anomalies decrease as temperature rises during a heatwave, indicating a moisture limitation; in tandem, sensible heat flux anomalies at the surface increase, further increasing near-surface air temperature. The trends are in the opposite direction for the Northeast and Northwest, although with a lesser relative magnitude. In response to additional heating in these regions, additional water is evaporated or transpired from the land surface, leading to an increase in latent heat flux anomalies. The decrease in sensible heat fluxes indicates that the ground is cooler than the overlying atmosphere for these heatwaves (not shown), highlighting the importance of processes like advection over soil moisture–mediated heating. While we do not explore the role of humidity in heatwaves here, the increase in latent heat in the energy-limited regimes will likely lead to increases in near-surface humidity, and therefore a higher heat index for a given temperature anomaly, assuming that the heatwave is not caused by advection of hot, dry air into the region.

To see the differing relationship between soil moisture and heatwaves for moisture versus energy limited regimes, Fig. 12 shows the progression of temperature anomalies, the estimated dynamical components (i.e., those temperature anomalies predicted by lead-1 SLP anomalies), and soil moisture anomalies for the South, Northeast, and Northwest from 31 days prior to the start of the heatwave through the end of the event. Heatwaves are split into the bottom and top quartile of residual component (the difference between the actual temperature anomaly and the dynamical component) magnitude and averaged. We would expect the high-residual events and the regions with stronger negative correlation between soil moisture anomalies and the residual component to demonstrate larger soil moisture deficits. This holds true, with the South experiencing larger soil moisture deficits before and during heatwaves than the Northwest and Northeast, as well as larger deficits in the high-residual events than low-residual cases in all regions. However, Fig. 12 also reveals a stark contrast in how long high-residual events last as compared with low-residual events in the moisture-limited (South) versus energy-limited (Northwest and Northeast) regions.

During low-residual events, in which the temperature anomalies during the heatwave week can be better predicted using SLP analogs, all three regions behave similarly. Temperature anomalies begin increasing one to two days prior to the start of the heatwave week, rising rapidly as the extreme heat-associated circulation pattern occurs, and peaking near 1.5 standard deviations above the climatological temperature. The behavior of the dynamical prediction is nearly identical, as expected. Significant soil moisture anomalies generally only occur during the heatwave week or a few days before, as

Unauthenticated | Downloaded 11/29/22 04:04 PM UTC

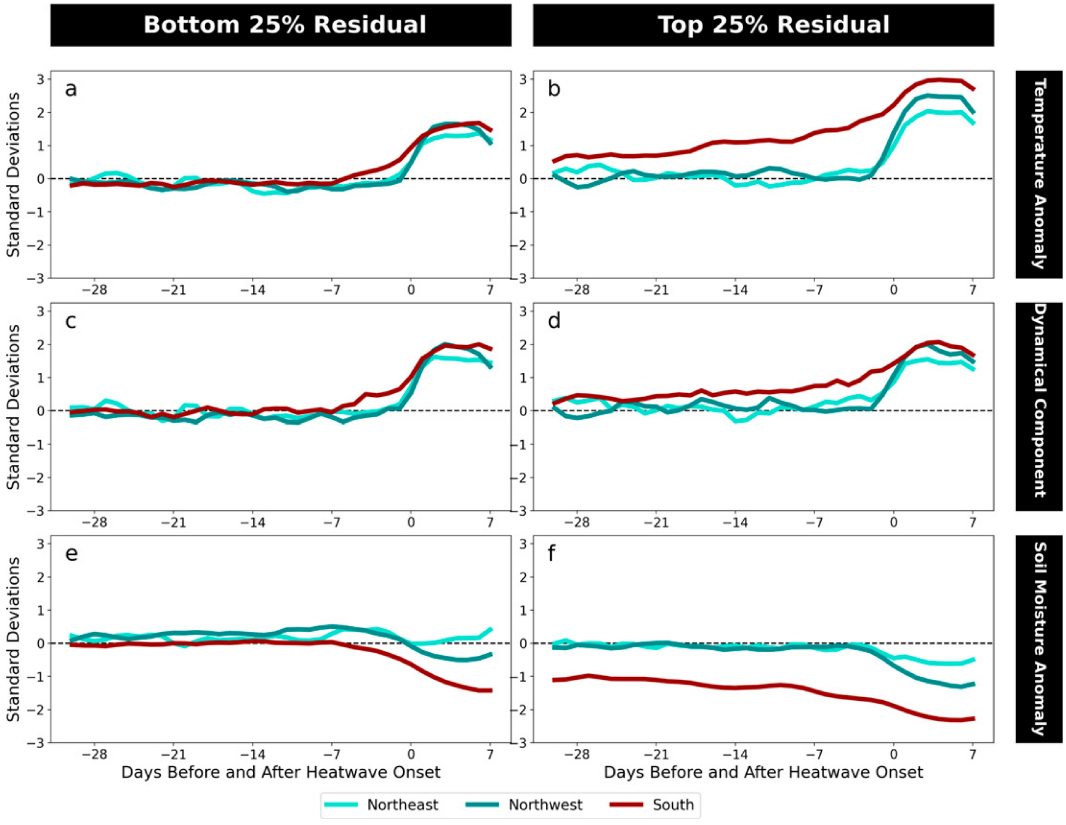

FIG. 12. Heatwave progression in three representative regions for heatwaves with residual components in the (left) lower quartile and (right) upper quartile of fully coupled preindustrial control simulation heatwaves, showing (a),(b) average temperature anomalies; (c),(d) average dynamical component; and (e),(f) average soil moisture anomalies for 31 days before the start of the heatwave (day 1) through the last day of the heatwave (day 7). The values are measured in standard deviations, which have been calculated for each region as the square root of the area-weighted average of the variances calculated for each summer individually. The dynamical component is measured in temperature standard deviation. The Northeast and Northwest are chosen to represent energy-limited regions, whereas the South is chosen to represent moisture-limited regions.

the elevated temperature leads to increased evapotranspiration from the surface.

On the other hand, there is a marked difference between the regions during high-residual events. The Northwest and Northeast behave largely the same as during low-residual events, but with greater magnitudes in the size of anomalies during the heatwave week. These regions again experience elevated temperature anomalies a few days before the heatwave week, but now increase in temperature more rapidly, peaking closer to 2 standard deviations. The dynamical component also increases a few days before, but only peaks at 1.5 standard deviations (by definition, a high residual event will have a discrepancy between its temperature anomaly and its dynamical component). The soil moisture again declines only during the week of the heatwave. The decrease in soil moisture is greater, likely due to the higher temperatures inducing more evapotranspiration.

In the South, there is very different behavior in the high-residual events than in the low-residual events. The peak heatwave temperature is 44% greater than the dynamically predicted temperature, in part due to the reduced latent heat fluxes and, therefore, enhanced surface heating, linked to the low soil moisture. Positive temperature anomalies and negative soil moisture anomalies extend back for the full 31-day period prior to the heatwave. While the rate of change in temperature does peak at the start of the heatwave week, the heatwave is building upon a long period of hot and dry conditions. These persistent hot and dry conditions are not entirely explained by circulation, as the temperature anomaly exceeds the dynamical component throughout the period. This indicates an important role for soil moisture preconditioning in the South: while we may not be able to predict a heatwave 31 days in advance, the presence of anomalously low soil moisture at that lead time would suggest that any future heatwave-associated circulation pattern will likely result in more extreme temperatures.

d. Future trends

Having identified the circulation patterns and soil moisture anomalies associated with extreme heat, we next explore

Unauthenticated | Downloaded 11/29/22 04:04 PM UTC

FIG. 13. By decade, percentage of days with a correlation above 0.4 between daily summer sea level pressure patterns in CESM1-LE and the average sea level pressure pattern for fully coupled preindustrial control simulation heatwaves. Statistically significant linear trend lines for 2010–99 are shown in red.

whether the probabilities of these heatwave ingredients are projected to change. To assess potential future changes, we use the CESM1-LE. Using all 40 ensemble members limits the impact of internal variability on the results, allowing a clearer picture of the forced response to human influence in the model.

Focusing first on projected forced circulation changes, we calculate the spatial correlation between each summer day in CESM1-LE and the average heatwave lead-1 SLP anomaly pattern from PiCTL (the patterns seen in Fig. 6). For each region, these correlations are calculated over the same expanded spatial domain that was used for the CCAs. The results, shown as the percentage of summer days per decade with a spatial correlation greater than 0.4, are plotted in Fig. 13. The cutoff of 0.4 is chosen because it is the mean correlation across all regions between lead-1 SLP anomalies during days in heatwaves and the average heatwave lead-1 SLP anomaly pattern. Controlling for a false discovery rate of 0.05, there is a statistically significant positive trend over the period 2010–99 in CESM1-LE in six of the nine regions and a statistically significant negative trend in two of the remaining three regions. For those regions with an increasing trend, the percentage is generally stable in the historical period, before increasing rapidly over the twenty-first century.

To further understand these increases, we define a heatwave-inducing circulation event as one or more consecutive days with SLP anomalies that have a correlation greater than 0.4 with the PiCTL heatwave pattern. For the regions with an increasing percentage of days exhibiting heatwave-inducing SLP patterns, we find that the increase is driven by both an increase in the number of separate events per year with the heatwave SLP patterns and an increase in event duration (Figs. S4 and S5 in the online supplemental material). This increasing trend in circulation events similar to those associated with heatwaves indicates a potential forced response in the dynamic controls on extreme heat. However, given that heatwaves

Unauthenticated | Downloaded 11/29/22 04:04 PM UTC

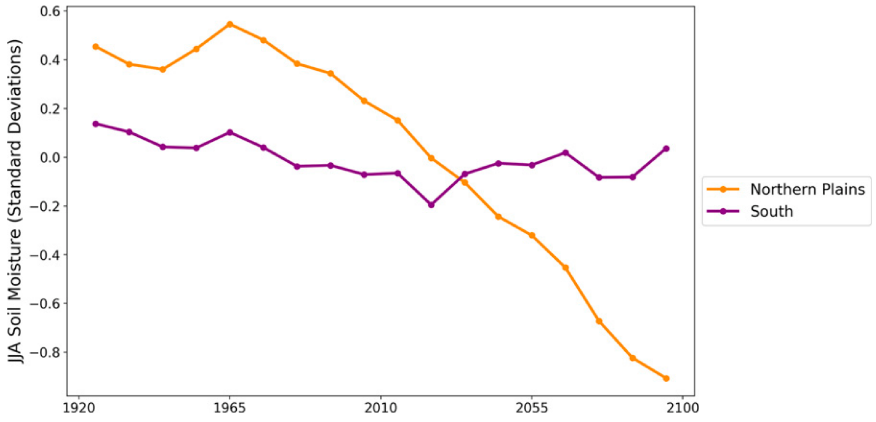

FIG. 14. By decade, average summer soil moisture in CESM1-LE for the South and Northern Plains regions. Soil moisture is measured in intrasummer fully coupled preindustrial control simulation soil moisture standard deviations. The mean and seasonal cycle have been removed with respect to the period 1920–2100 for each ensemble member.

can also influence SLP, this analysis alone cannot conclusively establish causation.

Previous studies have identified decreasing trends in future projections of soil moisture in the American West (Mankin et al. 2017), Southwest (Seager et al. 2013; Cook et al. 2015), and Central Plains (Cook et al. 2015). Here we focus on trends in soil moisture in the U.S. South and Northern Plains regions in the CESM1-LE, since these two regions displayed stronger links between the residual component of temperature and soil moisture anomalies. The trend in decadal average summer soil moisture for these two regions is displayed in Fig. 14. The values are measured in each region's intrasummer PiCTL soil moisture standard deviation.

No visible trend is present in the South, as mean summer soil moisture appears to remain relatively constant throughout the simulations. However, in the Northern Plains, there is a clear decreasing trend. From the 1920s to the 2050s, mean soil moisture decreases by over one-half of a standard deviation. By the 2100s, the decrease has surpassed a full standard deviation. Regressing the residual component on 1-week lagged soil moisture during Northern Plains heatwaves in the PiCTL provides a coefficient of −0.33°C per standard deviation of soil moisture change. From the baseline of mean soil moisture in 1920–2010, this implies a potential amplification of the residual component of 0.21°–0.41°C for 2040–49 and 2080–89, respectively, which could increase the severity of heatwaves in this region.

4. Discussion and conclusions

In this study we apply CCAs to daily summer temperature to estimate the contribution of concurrent atmospheric circulation to extreme heat events. As expected, we find that atmospheric circulation and accompanying processes explain the majority of temperature anomalies during heatwaves. We then explore the "residual component" (defined as the temperature anomaly unexplained by dynamical adjustment), which is largest in the central United States. In this region, 15%–25% of the heatwave temperature anomalies are not explained by the lead-1 circulation, and soil moisture is identified as having an important role in amplifying temperatures beyond that expected from heatwave-associated circulation alone. Further, we present evidence that during events with the largest residual component (which should roughly align with the most extreme events) in the central United States, negative soil moisture anomalies are present over a month in advance of the heatwave.

Before discussing the implications of these findings further, we note a number of caveats of our results. First, our analysis of a single model, CESM1, means that the results could reflect relationships that are not present in the true Earth system or other climate models; future work should establish consistency in other data sources. Second, we take advantage of long control simulations that both improve the skill of our CCA method and remove the need to account for nonstationarity related to human influence on the climate system. Applying the same technique we use here to observational data would be more difficult and result in a noisier estimate of the circulation-induced component of temperature, owing to the much shorter data record and the presence of an anthropogenic forced response. This highlights the need for further statistical advances in dynamical adjustment that can improve the signal-to-noise ratio, such as those explored in, for example, Sippel et al. (2019). Third, CCAs assume a linear relationship between SLP and temperature, which is likely a simplification of the true relationship. As such, a portion of the residual component that we attributed to nondynamical processes could instead reflect nonlinearities in the relationship between temperature and SLP. Further, SLP is not a complete descriptor of all components of the atmospheric circulation; future work could explore using multiple predictors, such as Z500 and advection, in addition to SLP. Fourth, we fix the domain size for SLP in advance of our dynamical adjustment procedure. While our decision is based on physical reasons (the ability to encapsulate wave-5 and higher wavenumber circulation patterns, which are often

Unauthenticated | Downloaded 11/29/22 04:04 PM UTC

associated with heatwaves), it will inherently include some subregions whose behavior is not relevant for temperature in the region. Future methodological developments could explore whether subsetting the domain based on, for example, S2N or other metrics of significance and consistency is statistically valid and improves performance. Fifth, the CCA method has an inherent dependence on the domains chosen for temperature, in addition to SLP. While our climate regions are sufficiently small that they are likely to experience heatwaves synchronously, it is possible that results could differ with different regions. We are nevertheless encouraged because Deser et al. (2016) found little sensitivity to domain size and because our results are similar to those of Merrifield et al. (2017), who dynamically adjusted the United States as a whole. Sixth, insofar as SLP is affected by the land surface (such as the effect of surface temperature on thermal low development), it is possible that some of the dynamical component that we estimate may be better attributed to the land and not to the circulation. As the land and atmosphere affect each other, we are not able to completely separate the two. Using many analogs to predict the circulation effect should reduce the land effect on the dynamical component, but it may still be present when there are extremely close links between certain land and atmospheric patterns. Replacing SLP with Z500 would not solve this issue of causality, as it too is affected by surface conditions. There may be other variables beyond 1-week lagged soil moisture that would help to explain the residual component in these regions.

Despite these limitations, our methodology provides a general framework with which to parse the dynamical components of heatwaves from those resulting from other processes. The approach confirms the central United States as a land–atmosphere coupling hot spot (e.g., Zhang et al. 2008; Merrifield et al. 2017; Vogel et al. 2017). In the South region, we find that negative soil moisture anomalies and positive dynamically predicted temperature anomalies precede the hottest heatwaves by over a month (recall Fig. 12). These anomalies suggest soil moisture as a source of heatwave predictability in the region and raise the possibility of positive feedbacks occurring between the land surface and the atmosphere as follows: The circulation patterns associated with positive dynamically predicted temperatures would be expected to lead to negative soil moisture anomalies. In addition, it is possible that negative soil moisture anomalies, via reducing evapotranspiration and increasing sensible heating, could have an effect on circulation patterns that drives an increase in the dynamical component of temperature. Such a positive feedback has been identified in Europe, where Miralles et al. (2014) showed that, during megaheatwaves, soil desiccation enhanced temperatures by increasing entrainment of warm air into the boundary layer and Haarsma et al. (2009) demonstrated that warm easterly winds were driven by drier soils. In North America, Teng et al. (2019) found that prescribing low soil water in CESM1 during the summer led to positive geopotential height anomalies over North America and drove a circumglobal teleconnection response. While these studies support the idea of land–atmosphere feedbacks causing the persistent hot and dry conditions we observed, it is also plausible that circulation patterns consistent with positive temperature anomalies and drier soils are particularly persistent in the central United States because of factors other than soil moisture feedbacks.

While soil moisture provided a consistent explanation for the amplification of heatwaves in the central United States, we did not find the same relationships for the remainder of the country. Circulation accounted for a larger proportion of temperature anomalies in the western and eastern United States than in the central United States, but the dynamical prediction typically failed to explain 5%–15% of the anomalies. If the residuals resulted from unbiased methodological error, we would expect that each event might have large positive or negative residuals, but on average they would be zero. The fact that the average dynamic component of temperature is always found to be less than the actual temperature anomaly indicates that there is a systematic underestimation. One explanation is that because we are filtering to particularly extreme events, the circulation patterns may be particularly distinct and possess fewer close analogs, leading to poorer prediction during these events. Given the large number of potential analogs in the CESM1 preindustrial simulation, this seems unlikely to fully explain the residual component. Other possibilities related to our CCA methodology are that SLP is an incomplete proxy for the atmospheric circulation, that the assumption of linearity between SLP and temperature does not hold for more extreme events, that the spatial domains used to define regions and perform CCA can be better defined, and/or that the time evolution of the circulation is relevant.

Looking to the future, the CESM1-LE projects an increase in the probability of the heatwave-associated circulation patterns that we identified in the PiCTL in six of nine regions, raising the possibility of a forced increase in heatwaves due to dynamical changes. However, from our analysis alone, the causality is unclear because some of the SLP patterns associated with heatwaves, such as thermal lows, could have been caused by the heatwaves themselves. Further, it is not guaranteed that the relationship between SLP and temperature is stationary. When dynamically adjusting the CESM1-LE using the PiCTL as SLP analogs (Deser et al. 2016) or dynamically adjusting observations, where history provides analogs, a trend in the distribution of SLP may make similar SLP events less analogous and reduce the utility of dynamical adjustment techniques.

Throughout our study, we used a fixed definition of a heatwave based on the 7-day average of daily average 2-m air temperature anomalies. We do not expect that our general results—the importance of the atmospheric circulation in explaining heat, the role of the land surface in the central United States, and the different evolution of sensible and latent heat fluxes during heatwaves in moisture versus energy limited regions—would change with other reasonable definitions of heatwaves. However, the specific evolution of the land–atmosphere system in advance of heatwaves will differ with other definitions, such as whether a heatwave is defined using daily minimum, maximum, or average temperatures (e.g., Bumbaco et al. 2013). While there is no single definition of a heatwave, different definitional decisions

Unauthenticated | Downloaded 11/29/22 04:04 PM UTC

have implications for the associated impacts of the extreme event. Thus, an interesting future direction is to use the framework developed here to systematically compare the atmospheric and land surface precursors with different metrics of heatwaves.

Overall, this study demonstrated the application and performance of CCAs to daily temperature data. Using this methodology with daily data expands the possibility to investigate extreme events that are relevant on shorter time scales. We demonstrated the presence of persistent soil moisture deficits and circulation anomalies in the most severe central U.S. heatwaves, suggesting a role of land–atmosphere coupling and feedbacks. Having developed and tested our framework using a large climate model dataset, it would be useful to extend this analysis to observational data. Doing so would require modifications to address additional sources of variability and uncertainty, because of the shorter data record and the role of anthropogenic climate change. In closing, inasmuch as there is a strong link to the circulation, this technique could be applied to other extremes, such as high-precipitation events and droughts.

Acknowledgments. We acknowledge the CESM1 Large Ensemble Community Project and the computing resources provided by NCAR's Computational and Information Systems Laboratory, including the Cheyenne supercomputer (doi: 10.5065/D6RX99HX). Author Horowitz was supported in part by NRT-INFEWS: Integrated Urban Solutions for Food, Energy, and Water Management (Grant DGE-1735325) and the National Science Foundation (Grant AGS-1939988). Author McKinnon was supported in part by the National Science Foundation (Grant AGS-1939988). Author Simpson is supported by the National Center for Atmospheric Research, which is a major facility sponsored by the National Science Foundation under the Cooperative Agreement 1852977.

Data availability statement. The CESM1 control runs and CESM1-LE data can be found at NCAR's Climate Data Gateway (https://doi.org/10.5065/d6j101d1). The code for reproducing this analysis is available online (https://github.com/russellhz/extreme_heat_CCA).

REFERENCES

Adams, R. E., C. C. Lee, E. T. Smith, and S. C. Sheridan, 2021: The relationship between atmospheric circulation patterns and extreme temperature events in North America. *Int. J. Climatol.*, **41**, 92–103, https://doi.org/10.1002/joc.6610.

Anderson, B. G., and M. L. Bell, 2009: Weather-related mortality: How heat, cold, and heat waves affect mortality in the United States. *Epidemiology*, **20**, 205–213, https://doi.org/10.1097/EDE.0b013e318190ee08.

Benjamini, Y., and Y. Hochberg, 1995: Controlling the false discovery rate: A practical and powerful approach to multiple testing. *J. Roy. Stat. Soc.*, **57B**, 289–300, https://doi.org/10.1111/j.2517-6161.1995.tb02031.x.

Bumbaco, K. A., K. D. Dello, and N. A. Bond, 2013: History of Pacific Northwest heat waves: Synoptic pattern and trends. *J. Appl. Meteor. Climatol.*, **52**, 1618–1631, https://doi.org/10.1175/JAMC-D-12-094.1.

Cook, B. I., T. R. Ault, and J. E. Smerdon, 2015: Unprecedented 21st century drought risk in the American Southwest and Central Plains. *Sci. Adv.*, **1**, e1400082, https://doi.org/10.1126/sciadv.1400082.

Coumou, D., V. Petoukhov, S. Rahmstorf, S. Petri, and H. J. Schellnhuber, 2014: Quasi-resonant circulation regimes and hemispheric synchronization of extreme weather in boreal summer. *Proc. Natl. Acad. Sci. USA*, **111**, 12 331–12 336, https://doi.org/10.1073/pnas.1412797111.

Deser, C., L. Terray, and A. S. Phillips, 2016: Forced and internal components of winter air temperature trends over North America during the past 50 years: Mechanisms and implications. *J. Climate*, **29**, 2237–2258, https://doi.org/10.1175/JCLI-D-15-0304.1.

Fischer, E. M., S. I. Seneviratne, D. Lüthi, and C. Schär, 2007a: Contribution of land–atmosphere coupling to recent European summer heat waves. *Geophys. Res. Lett.*, **34**, L06707, https://doi.org/10.1029/2006GL029068.

——, ——, P. L. Vidale, D. Lüthi, and C. Schär, 2007b: Soil moisture–atmosphere interactions during the 2003 European summer heat wave. *J. Climate*, **20**, 5081–5099, https://doi.org/10.1175/JCLI4288.1.

Gasparrini, A., and Coauthors, 2015: Mortality risk attributable to high and low ambient temperature: A multicountry observational study. *Lancet*, **386**, 369–375, https://doi.org/10.1016/S0140-6736(14)62114-0.

Gershunov, A., D. R. Cayan, and S. F. Iacobellis, 2009: The great 2006 heat wave over California and Nevada: Signal of an increasing trend. *J. Climate*, **22**, 6181–6203, https://doi.org/10.1175/2009JCLI2465.1.

Goodman, J., M. Hurwitz, J. Park, and J. Smith, 2018: Heat and learning. National Bureau of Economic Research Working Paper 24639, 60 pp., https://doi.org/10.3386/w24639.

Grotjahn, R., and Coauthors, 2016: North American extreme temperature events and related large scale meteorological patterns: A review of statistical methods, dynamics, modeling, and trends. *Climate Dyn.*, **46**, 1151–1184, https://doi.org/10.1007/s00382-015-2638-6.

Guirguis, K., A. Gershunov, A. Tardy, and R. Basu, 2014: The impact of recent heat waves on human health in California. *J. Appl. Meteor. Climatol.*, **53**, 3–19, https://doi.org/10.1175/JAMC-D-13-0130.1.

Haarsma, R. J., F. Selten, B. Hurk, W. Hazeleger, and X. Wang, 2009: Drier Mediterranean soils due to greenhouse warming bring easterly winds over summertime central Europe. *Geophys. Res. Lett.*, **36**, L04705, https://doi.org/10.1029/2008GL036617.

Hauser, M., R. Orth, and S. I. Seneviratne, 2016: Role of soil moisture versus recent climate change for the 2010 heat wave in western Russia. *Geophys. Res. Lett.*, **43**, 2819–2826, https://doi.org/10.1002/2016GL068036.

Heal, G., and J. Park, 2016: Temperature stress and the direct impact of climate change: A review of an emerging literature. *Rev. Environ. Econ. Policy*, **10**, 347–362, https://doi.org/10.1093/reep/rew007.

Hirschi, M., and Coauthors, 2011: Observational evidence for soil-moisture impact on hot extremes in southeastern Europe. *Nat. Geosci.*, **4**, 17–21, https://doi.org/10.1038/ngeo1032.

Unauthenticated | Downloaded 11/29/22 04:04 PM UTC

Honda, Y., and Coauthors, 2014: Heat-related mortality risk model for climate change impact projection. *Environ. Health Prev. Med.*, **19**, 56–63, https://doi.org/10.1007/s12199-013-0354-6.

Horton, R. M., J. S. Mankin, C. Lesk, E. Coffel, and C. Raymond, 2016: A review of recent advances in research on extreme heat events. *Curr. Climate Change Rep.*, **2**, 242–259, https://doi.org/10.1007/s40641-016-0042-x.

Hurrell, J. W., and Coauthors, 2013: The Community Earth System Model: A framework for collaborative research. *Bull. Amer. Meteor. Soc.*, **94**, 1339–1360, https://doi.org/10.1175/BAMS-D-12-00121.1.

Jaeger, E. B., and S. I. Seneviratne, 2011: Impact of soil moisture–atmosphere coupling on European climate extremes and trends in a regional climate model. *Climate Dyn.*, **36**, 1919–1939, https://doi.org/10.1007/s00382-010-0780-8.

Karl, T. R., and W. J. Koss, 1984: Regional and national monthly, seasonal, and annual temperature weighted by area 1895–1983. NOAA Historical Climate Series 4-3, 8 pp., https://repository.library.noaa.gov/view/noaa/10238.

Kay, J. E., and Coauthors, 2015: The Community Earth System Model (CESM) large ensemble project: A community resource for studying climate change in the presence of internal climate variability. *Bull. Amer. Meteor. Soc.*, **96**, 1333–1349, https://doi.org/10.1175/BAMS-D-13-00255.1.

Kjellstrom, T., R. S. Kovats, S. J. Lloyd, T. Holt, and R. S. J. Tol, 2009: The direct impact of climate change on regional labor productivity. *Arch. Environ. Occup. Health*, **64**, 217–227, https://doi.org/10.1080/19338240903352776.

Kornhuber, K., S. Osprey, D. Coumou, S. Petri, V. Petoukhov, S. Rahmstorf, and L. Gray, 2019: Extreme weather events in early summer 2018 connected by a recurrent hemispheric wave-7 pattern. *Environ. Res. Lett.*, **14**, 054002, https://doi.org/10.1088/1748-9326/ab13bf.

——, D. Coumou, E. Vogel, C. Lesk, J. F. Donges, J. Lehmann, and R. M. Horton, 2020: Amplified Rossby waves enhance risk of concurrent heatwaves in major breadbasket regions. *Nat. Climate Change*, **10**, 48–53, https://doi.org/10.1038/s41558-019-0637-z.

Koster, R. D., and M. J. Suarez, 2001: Soil moisture memory in climate models. *J. Hydrometeor.*, **2**, 558–570, https://doi.org/10.1175/1525-7541(2001)002%3C0558:SMMICM%3E2.0.CO;2.

Kretschmer, M., J. Cohen, V. Matthias, J. Runge, and D. Coumou, 2018: The different stratospheric influence on cold-extremes in Eurasia and North America. *npj Climate Atmos. Sci.*, **1**, 44, https://doi.org/10.1038/s41612-018-0054-4.

Lau, N.-C., and M. J. Nath, 2012: A model study of heat waves over North America: Meteorological aspects and projections for the twenty-first century. *J. Climate*, **25**, 4761–4784, https://doi.org/10.1175/JCLI-D-11-00575.1.

Lehner, F., C. Deser, and L. Terray, 2017: Toward a new estimate of "time of emergence" of anthropogenic warming: Insights from dynamical adjustment and a large initial-condition model ensemble. *J. Climate*, **30**, 7739–7756, https://doi.org/10.1175/JCLI-D-16-0792.1.

——, ——, I. R. Simpson, and L. Terray, 2018: Attributing the U.S. Southwest's recent shift into drier conditions. *Geophys. Res. Lett.*, **45**, 6251–6261, https://doi.org/10.1029/2018GL078312.

Lo, M.-H., T.-H. Kuo, H.-W. Wey, C.-W. Lan, and J.-P. Chen, 2017: Land processes as the forcing of extremes. *Climate Extremes*: *Patterns and Mechanisms*, *Geophys. Monogr.*, Vol. 226, Amer. Geophys. Union, 75–92, https://doi.org/10.1002/9781119068020.ch5.

Loikith, P. C., and A. J. Broccoli, 2012: Characteristics of observed atmospheric circulation patterns associated with temperature extremes over North America. *J. Climate*, **25**, 7266–7281, https://doi.org/10.1175/JCLI-D-11-00709.1.

Lorenz, R., E. B. Jaeger, and S. I. Seneviratne, 2010: Persistence of heat waves and its link to soil moisture memory. *Geophys. Res. Lett.*, **37**, L09703, https://doi.org/10.1029/2010GL042764.

Mankin, J. S., J. E. Smerdon, B. I. Cook, A. P. Williams, and R. Seager, 2017: The curious case of projected twenty-first-century drying but greening in the American west. *J. Climate*, **30**, 8689–8710, https://doi.org/10.1175/JCLI-D-17-0213.1.

McKinnon, K. A., A. Rhines, M. P. Tingley, and P. Huybers, 2016: Long-lead predictions of eastern United States hot days from Pacific sea surface temperatures. *Nat. Geosci.*, **9**, 389–394, https://doi.org/10.1038/ngeo2687.

Meehl, G. A., and C. Tebaldi, 2004: More intense, more frequent, and longer lasting heat waves in the 21st century. *Science*, **305**, 994–997, https://doi.org/10.1126/science.1098704.

Merrifield, A., F. Lehner, S.-P. Xie, and C. Deser, 2017: Removing circulation effects to assess central U.S. land–atmosphere interactions in the CESM large ensemble. *Geophys. Res. Lett.*, **44**, 9938–9946, https://doi.org/10.1002/2017GL074831.

——, I. R. Simpson, K. A. McKinnon, S. Sippel, S.-P. Xie, and C. Deser, 2019: Local and nonlocal land surface influence in European heatwave initial condition ensembles. *Geophys. Res. Lett.*, **46**, 14 082–14 092, https://doi.org/10.1029/2019GL083945.

Miralles, D. G., A. J. Teuling, C. C. van Heerwaarden, and J. V.-G. de Arellano, 2014: Mega-heatwave temperatures due to combined soil desiccation and atmospheric heat accumulation. *Nat. Geosci.*, **7**, 345–349, https://doi.org/10.1038/ngeo2141.

——, P. Gentine, S. I. Seneviratne, and A. J. Teuling, 2019: Land–atmospheric feedbacks during droughts and heatwaves: State of the science and current challenges. *Ann. N. Y. Acad. Sci.*, **1436**, 19–35, https://doi.org/10.1111/nyas.13912.

Moore, F. C., N. Obradovich, F. Lehner, and P. Baylis, 2019: Rapidly declining remarkability of temperature anomalies may obscure public perception of climate change. *Proc. Natl. Acad. Sci. USA*, **116**, 4905–4910, https://doi.org/10.1073/pnas.1816541116.

Mueller, B., and S. I. Seneviratne, 2012: Hot days induced by precipitation deficits at the global scale. *Proc. Natl. Acad. Sci. USA*, **109**, 12 398–12 403, https://doi.org/10.1073/pnas.1204330109.

Pfahl, S., and H. Wernli, 2012: Quantifying the relevance of atmospheric blocking for co-located temperature extremes in the Northern Hemisphere on (sub-)daily time scales. *Geophys. Res. Lett.*, **39**, L12807, https://doi.org/10.1029/2012GL052261.

Romero-Lankao, P., J. Smith, D. Davidson, N. Diffenbaugh, P. Kinney, P. Kirshen, P. Kovacs, and L. V. Ruiz, 2014: North America. *Climate Change 2014: Impacts, Adaptation, and Vulnerability. Part B: Regional Aspects.* V. Barros et al., Eds., Cambridge University Press, 1439–1498.

Röthlisberger, M., L. Frossard, L. F. Bosart, D. Keyser, and O. Martius, 2019: Recurrent synoptic-scale Rossby wave patterns and their effect on the persistence of cold and hot spells. *J. Climate*, **32**, 3207–3226, https://doi.org/10.1175/JCLI-D-18-0664.1.

Sánchez, B., A. Rasmussen, and J. R. Porter, 2014: Temperatures and the growth and development of maize and rice: A review. *Global Change Biol.*, **20**, 408–417, https://doi.org/10.1111/gcb.12389.

Schlenker, W., and M. J. Roberts, 2009: Nonlinear temperature effects indicate severe damages to U.S. crop yields under

Unauthenticated | Downloaded 11/29/22 04:04 PM UTC

climate change. *Proc. Natl. Acad. Sci. USA*, **106**, 15 594–15 598, https://doi.org/10.1073/pnas.0906865106.

Schubert, S., H. Wang, and M. Suarez, 2011: Warm season subseasonal variability and climate extremes in the Northern Hemisphere: The role of stationary Rossby waves. *J. Climate*, **24**, 4773–4792, https://doi.org/10.1175/JCLI-D-10-05035.1.

Screen, J. A., and I. Simmonds, 2014: Amplified mid-latitude planetary waves favour particular regional weather extremes. *Nat. Climate Change*, **4**, 704–709, https://doi.org/10.1038/nclimate2271.

Seager, R., M. Ting, C. Li, N. Naik, B. Cook, J. Nakamura, and H. Liu, 2013: Projections of declining surface-water availability for the southwestern United States. *Nat. Climate Change*, **3**, 482–486, https://doi.org/10.1038/nclimate1787.

Selten, F. M., R. Bintanja, R. Vautard, and B. J. J. M. van den Hurk, 2020: Future continental summer warming constrained by the present-day seasonal cycle of surface hydrology. *Sci. Rep.*, **10**, 4721, https://doi.org/10.1038/s41598-020-61721-9.

Seneviratne, S. I., and Coauthors, 2006: Soil moisture memory in AGCM simulations: Analysis of Global Land–Atmosphere Coupling Experiment (GLACE) data. *J. Hydrometeor.*, **7**, 1090–1112, https://doi.org/10.1175/JHM533.1.

——, T. Corti, E. L. Davin, M. Hirschi, E. B. Jaeger, I. Lehner, B. Orlowsky, and A. J. Teuling, 2010: Investigating soil moisture–climate interactions in a changing climate: A review. *Earth-Sci. Rev.*, **99**, 125–161, https://doi.org/10.1016/j.earscirev.2010.02.004.

——, and Coauthors, 2013: Impact of soil moisture–climate feedbacks on CMIP5 projections: First results from the GLACE-CMIP5 experiment. *Geophys. Res. Lett.*, **40**, 5212–5217, https://doi.org/10.1002/grl.50956.

Sillmann, J., V. V. Kharin, X. Zhang, F. W. Zwiers, and D. Bronaugh, 2013: Climate extremes indices in the CMIP5 multimodel ensemble: Part 1. Model evaluation in the present climate. *J. Geophys. Res. Atmos.*, **118**, 1716–1733, https://doi.org/10.1002/jgrd.50203.

Sippel, S., N. Meinshausen, A. Merrifield, F. Lehner, A. G. Pendergrass, E. Fischer, and R. Knutti, 2019: Uncovering the forced climate response from a single ensemble member using statistical learning. *J. Climate*, **32**, 5677–5699, https://doi.org/10.1175/JCLI-D-18-0882.1.

Song, X., S. Wang, Y. Hu, M. Yue, T. Zhang, Y. Liu, J. Tian, and K. Shang, 2017: Impact of ambient temperature on morbidity and mortality: An overview of reviews. *Sci. Total Environ.*, **586**, 241–254, https://doi.org/10.1016/j.scitotenv.2017.01.212.

Stéfanon, M., P. Drobinski, F. D'Andrea, C. Lebeaupin-Brossier, and S. Bastin, 2014: Soil moisture–temperature feedbacks at meso-scale during summer heat waves over western Europe. *Climate Dyn.*, **42**, 1309–1324, https://doi.org/10.1007/s00382-013-1794-9.

Taylor, K. E., R. J. Stouffer, and G. A. Meehl, 2012: An overview of CMIP5 and the experiment design. *Bull. Amer. Meteor. Soc.*, **93**, 485–498, https://doi.org/10.1175/BAMS-D-11-00094.1.

Teng, H., G. Branstator, H. Wang, G. A. Meehl, and W. M. Washington, 2013: Probability of US heat waves affected by a subseasonal planetary wave pattern. *Nat. Geosci.*, **6**, 1056–1061, https://doi.org/10.1038/ngeo1988.

——, ——, A. B. Tawfik, and P. Callaghan, 2019: Circumglobal response to prescribed soil moisture over North America. *J. Climate*, **32**, 4525–4545, https://doi.org/10.1175/JCLI-D-18-0823.1.

Teuling, A. J., and Coauthors, 2009: A regional perspective on trends in continental evaporation. *Geophys. Res. Lett.*, **36**, L02404, https://doi.org/10.1029/2008GL036584.

Thomas, N. P., M. G. Bosilovich, A. B. M. Collow, R. D. Koster, S. D. Schubert, A. Dezfuli, and S. P. Mahanama, 2020: Mechanisms associated with daytime and nighttime heat waves over the contiguous United States. *J. Appl. Meteor. Climatol.*, **59**, 1865–1882, https://doi.org/10.1175/JAMC-D-20-0053.1.

Vargas Zeppetello, L. R., E. Tétreault-Pinard, D. S. Battisti, and M. B. Baker, 2020: Identifying the sources of continental summertime temperature variance using a diagnostic model of land–atmosphere interactions. *J. Climate*, **33**, 3547–3564, https://doi.org/10.1175/JCLI-D-19-0276.1.

Vogel, E., M. G. Donat, L. V. Alexander, M. Meinshausen, D. K. Ray, D. Karoly, N. Meinshausen, and K. Frieler, 2019: The effects of climate extremes on global agricultural yields. *Environ. Res. Lett.*, **14**, 054010, https://doi.org/10.1088/1748-9326/ab154b.

Vogel, M. M., R. Orth, F. Cheruy, S. Hagemann, R. Lorenz, B. J. J. M. van den Hurk, and S. I. Seneviratne, 2017: Regional amplification of projected changes in extreme temperatures strongly controlled by soil moisture–temperature feedbacks. *Geophys. Res. Lett.*, **44**, 1511–1519, https://doi.org/10.1002/2016GL071235.

Vose, R., D. Easterling, K. Kunkel, A. LeGrande, and M. Wehner, 2017: Temperature changes in the United States. *Climate Science Special Report: Fourth National Climate Assessment*, Vol. I, D. J. Wuebbles et al., Eds., U.S. Global Change Research Program, 185–206, https://doi.org/10.7930/J0N29V45.

Wehrli, K., B. P. Guillod, M. Hauser, M. Leclair, and S. I. Seneviratne, 2019: Identifying key driving processes of major recent heat waves. *J. Geophys. Res. Atmos.*, **124**, 11 746–11 765, https://doi.org/10.1029/2019JD030635.

Yang, Z., F. Dominguez, and X. Zeng, 2019: Large and local-scale features associated with heat waves in the United States in reanalysis products and the NARCCAP model ensemble. *Climate Dyn.*, **52**, 1883–1901, https://doi.org/10.1007/s00382-018-4414-x.

Ye, X., R. Wolff, W. Yu, P. Vaneckova, X. Pan, and S. Tong, 2012: Ambient temperature and morbidity: A review of epidemiological evidence. *Environ. Health Perspect.*, **120**, 19–28, https://doi.org/10.1289/ehp.1003198.

Zhang, J., W.-C. Wang, and L. R. Leung, 2008: Contribution of land–atmosphere coupling to summer climate variability over the contiguous United States. *J. Geophys. Res.*, **113**, D22109, https://doi.org/10.1029/2008JD010136.

Unauthenticated | Downloaded 11/29/22 04:04 PM UTC